AIP | Journal of Applied Physics

Enhanced electron field emission properties by tuning the microstructure of ultrananocrystalline diamond film

Hsiu-Fung Cheng, Horng-Yi Chiang, Chuang-Chi Horng, Huang-Chin Chen, Chuan-Sheng Wang, and I-Nan Lin

Citation: Journal of Applied Physics **109**, 033711 (2011); doi: 10.1063/1.3544482
View online: http://dx.doi.org/10.1063/1.3544482
View Table of Contents: http://scitation.aip.org/content/aip/journal/jap/109/3?ver=pdfcov
Published by the AIP Publishing

Enhanced electron field emission properties by tuning the microstructure of ultrananocrystalline diamond film

Hsiu-Fung Cheng,[1] Horng-Yi Chiang,[1] Chuang-Chi Horng,[1] Huang-Chin Chen,[2] Chuan-Sheng Wang,[2,3] and I-Nan Lin[2,a)]
[1]*Department of Physics, National Taiwan Normal University, Taipei 116, Taiwan, Republic of China*
[2]*Department of Physics, Tamkang University, Tamsui 251, Taiwan, Republic of China*
[3]*Technology and Science Institute of Northern Taiwan, Peitou, 112 Taipei, Taiwan, Republic of China*

(Received 12 November 2010; accepted 11 December 2010; published online 4 February 2011)

Synthesis of microcrystalline-ultrananocrystalline composite diamond (MCD-UNCD) films, which exhibit marvelous electron field emission (EFE) properties, was reported. The EFE of MCD-UNCD composite diamond film can be turned on at a low field as 6.5 $V/\mu m$ and attain large EFE current density about 1.0 mA/cm^2 at 30 $V/\mu m$ applied field, which is better than the EFE behavior of the nondoped planar diamond films ever reported. The MCD-UNCD films were grown by a two-step microwave plasma enhanced chemical vapor deposition (MPECVD) process, including forming an UNCD layer in CH_4/Ar plasma that contains no extra H_2, followed by growing MCD layer using $CH_4/H_2/Ar$ plasma that contains large proportion of H_2. Microstructure examinations using high resolution transmission electron microscopy shows that the secondary MPECVD process modifies the granular structure of the UNCD layer, instead of forming a large grain diamond layer on top of UNCD films. The MCD-UNCD composite diamond films consist of numerous ultrasmall grains (~5 nm in size), surrounding large grains about hundreds of nanometer in size. Moreover, there exist abundant nanographites in the interfacial region between the grains that were presumed to form interconnected channels for electron transport, resulting in superior EFE properties for MCD-UNCD composite films. © *2011 American Institute of Physics*. [doi:10.1063/1.3544482]

I. INTRODUCTION

The synthesis of ultrananocrystalline diamond (UNCD) films with nanosized grains has attracted tremendous attention recently, since the UNCD films possess many excellent properties and several of them actually exceed those of conventional diamond with micron-sized grains.[1–5] As the grain size in UNCD film decreases smaller than 10 nm, surface smoothness increases markedly, making it possible for directly fabricating the devices.[6] Additionally, the decrease in diamond grain size increases the proportion of grain boundaries, which contain nondiamond carbon in the films and result in significant improvement in electrical properties. A very high electron field emission (EFE) characteristic has been reported for UNCD films.[7–10] The nondiamond contents and the crystal size of diamond grains in the films play a crucial role in the applications for electron field emitters. The incorporation of N_2-species into grain boundaries of UNCD films was observed to improve tremendously the electrical conductivity and, thereafter, the EFE characteristics for the films.[11,12] The limitation of such a process is that high substrate temperature (>800 °C) is required for efficiently incorporating the N_2 into the UNCD materials. Doping Li-species into UNCD by solid state diffusion process can efficiently convert the UNCD films into conductive at lower substrate temperature (<500 °C)[13] but such a process is limited by the availability of large size Li-containing substrate (in this case, $LiNbO_3$). In previous report,[14,15] we used a layer of UNCD as nuclei and successfully synthesized a diamond film with very unique granular structure that enhanced EFE properties. Such a process required neither substrate heating process (plasma heating in chemical vapor deposition process is sufficient) nor specialized Li-containing substrates and has tremendous potential for practical application. However, how such a granular structure was formed and how the EFE process was enhanced are not totally clear.

In this paper, we synthesize a composite diamond films using a modified process, i.e., we grew UNCD layer in Ar/CH_4 plasma to serve as nucleation layer and then grew diamond films on the UNCD layer in $Ar/H_2/CH_4$ plasma, which contains large proportion of H_2. Moreover, the Ar/H_2 ratio for growing the second diamond layer was varied systematically so as to optimize the microstructure of the composite films for enhancing their EFE properties. The microstructure development of these films was examined by using transmission electron microscopy (TEM) and a model was proposed based on the observations to explain the source of enhancement on the EFE properties.

II. EXPERIMENTAL

The diamond films were grown by a two-step microwave plasma enhanced chemical vapor deposition (MPECVD) process on n-type mirror polished Si (100) substrates. First, we grew a UNCD nucleation layer on Si substrates. The substrates were first ultrasonicated in a solution containing diamond powders (~1 nm) for 30 min and were ultrasonically cleaned by acetone to remove any adhered particles. UNCD diamond nuclei were then formed by the MPECVD process in Ar/CH_4 (2%) plasma for 60 min, using an IPLAS

a)Electronic mail: inanlin@mail.tku.edu.tw.

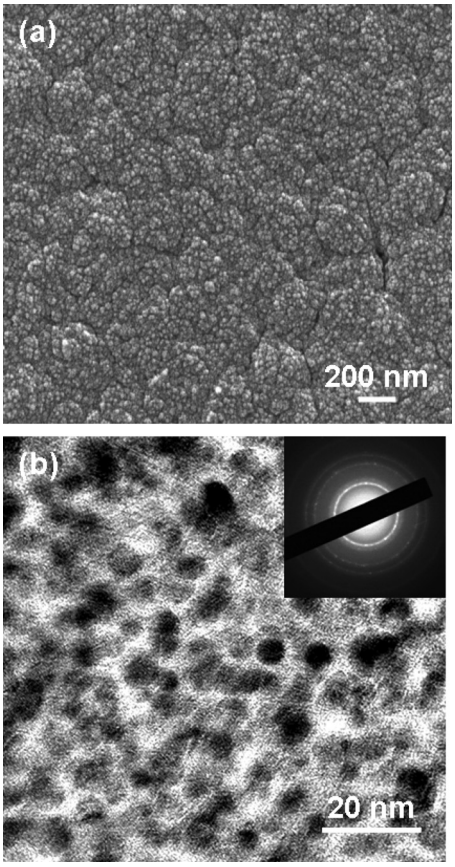

FIG. 1. (a) SEM and (b) TEM micrographs for the UNCD nucleation layer which were grown in $CH_4/H_2/Ar=4/0/196$ SCCM plasma for 60 min.

CYRANNUS-I system. Figure 1(a) shows the scanning electron microscopic (SEM) micrograph of the UNCD seeding layer, which consists of ultrasmall clusters. TEM micrograph of these UNCD seeding layer [Fig. 1(b)] and the associated selected area electron diffraction pattern [SAED, insets, Fig. 1(b)], reveals that the clusters contained in the seeding layer are ultrasmall diamond grains (~5 nm) with very uniform size distribution. There exists a thin layer (~1 nm) of amorphous carbons (a-C) along the grain boundaries of these nucleation layers. The significance of such an a-C layer will be discussed shortly. In the first series of MCD-UNCD composite films, the growth of second diamond layer was carried out in the same MPECVD process (2.45 GHz, IPLAS CYRANNUS-I) for 60 min with $CH_4/H_2/Ar=1/(99-x)/x$ SCCM (SCCM denotes cubic centimeter per minute at STP), where $x=0$, 25, 50, 75, and 90 and the films were designated as MCD-$UNCD_1$, MCD-$UNCD_2$, MCD-$UNCD_3$, MCD-$UNCD_4$, and MCD-$UNCD_5$, respectively (as listed in Table I). In the second series of composite films, the microdiamond films (MCD) were grown in a $CH_4/H_2/Ar=1/49/50$ SCCM plasma for different interval (30, 60, or 90 min). Thus obtained films were designated as MCD-$UNCD_{30}$, MCD-$UNCD_{60}$, and MCD-$UNCD_{90}$, respectively.

Surface morphology of nanodiamond films was examined using a field emission SEM (VEGA-TESCAN) and the microstructure of the films was examined using TEM (JOEL, 2100). Crystal quality of nanodiamond films was investigated by Raman spectroscopy using 325 nm laser beam (Renishaw). EFE properties of the diamond films were measured with a tunable parallel plate setup, in which the sample-to-anode distance was controlled using a micrometer. The current-voltage (*I-V*) characteristics were measured using an electrometer (Keithley 237) under pressures below 10^{-6} Torr. The EFE parameters were extracted from the obtained *I-V* curves by using the Fowler–Nordheim (FN) model.[16] The turn-on field (E_0) was designated as the intersection of the lines extrapolated from the low field and high field segments of the FN plot.

III. RESULTS AND DISCUSSION

Initially, the purpose of using UNCD as nucleation layer is to circumvent the presence of amorphous carbon prior to the formation of diamond nuclei. But, surprisingly, such a two-step process results in a film with completely different granular structure. The SEM morphology of MCD-UNCD composite films that were grown on UNCD nucleation layer is shown in Fig. 2, indicating that all of the MCD-UNCD

TABLE I. The MPECVD parameters (microwave power, pressure, $CH_4/H_2/Ar$ ratio, and growth time) used for growing the nucleation and MCD layers and the related turn-on field in EFE process for thus grown MCD-UNCD films.

		Nucleation layer[a]		MCD[b]		
	Samples	Gas composition ($CH_4/H_2/Ar$)	Growth time (min)	Gas composition ($CH_4/H_2/Ar$)	Growth time (min)	E_0 (V/μm)
	UNCD	4/0/196	60	···		17.6
	MCD	···		1/49/50		27.0
Series A	MCD-$UNCD_1$	4/0/196	60	1/99/00	60	23.2
	MCD-$UNCD_2$			1/94/25		12.7
	MCD-$UNCD_3$			1/49/50		6.5
	MCD-$UNCD_4$			1/24/75		15.3
	MCD-$UNCD_5$			1/09/90		17.3
Series B	MCD-$UNCD_{30}$	4/0/196	60	1/49/50	30	10.67
	MCD-$UNCD_{60}$				60	6.5
	MCD-$UNCD_{90}$				90	10.86

[a]The nucleation layers were grown in CH_4/Ar plasma with 1200 W/150 torr.
[b]The MCD layer were grown in $CH_4/H_2/Ar$ plasma with 1400 W/55 torr.

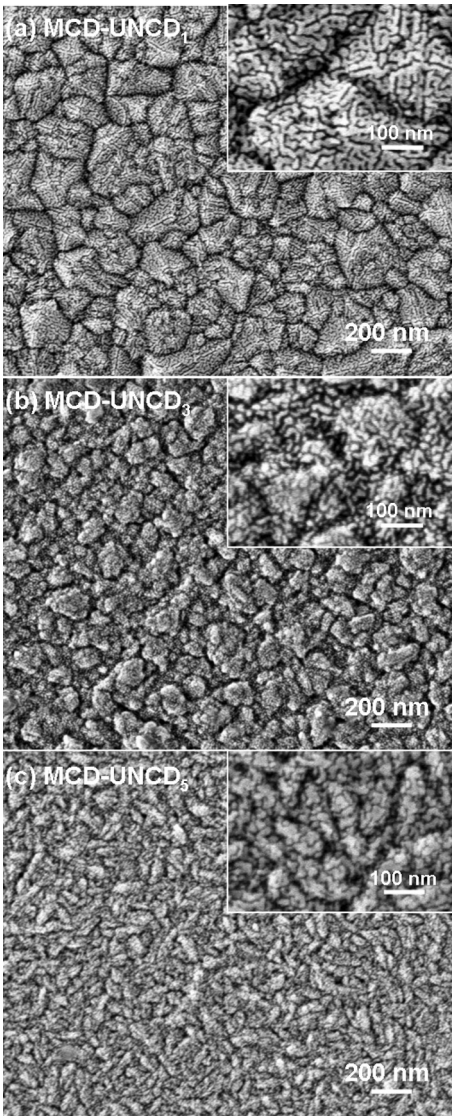

FIG. 2. SEM morphologies for MCD-UNCD composite diamond films grown on UNCD nucleation layer. The MCD layers were grown in $CH_4/H_2/Ar=1/(99-x)/x$ SCCM plasma with x=(a) 0 SCCM (MCD-UNCD$_1$), (b) 50 SCCM (MCD-UNCD$_3$), and (c) 90 SCCM (MCD-UNCD$_5$) for 60 min.

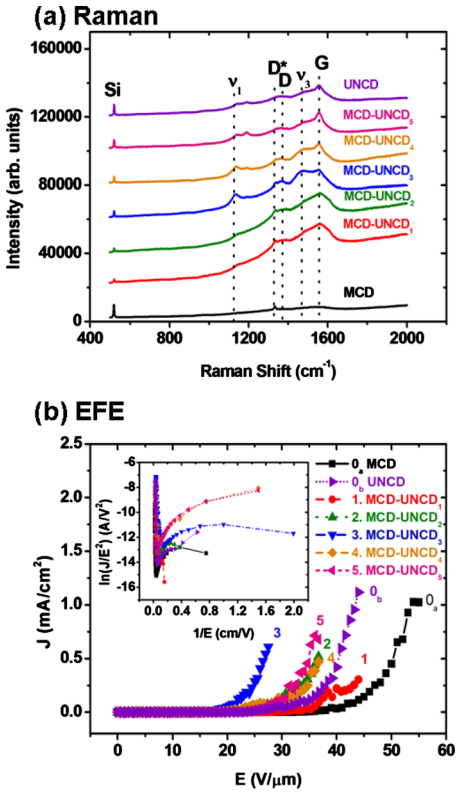

FIG. 3. (Color online) (a) Raman spectroscopy and (b) EFE properties for MCD-UNCD composite diamond films grown on UNCD nucleation layer. The MCD layers were grown in $CH_4/H_2/Ar=1/(99-x)/x$ SCCM plasma for 60 min (with x=0, 25, 50, 75, or 90 SCCM). Those for UNCD and MCD films that were grown in $CH_4/H_2/Ar=1/0/99$ or 1/99/0 SCCM plasma, respectively, were also included to facilitate the comparison.

films contain cauliflower geometry, i.e., there exist numerous tiny structures on large aggregates, which are more clearly illustrated as inset in Fig. 2. The large aggregates were uniformly distributed over the samples. The size of large aggregates, ~100–200 nm for MCD-UNCD$_1$ films [Fig. 2(a)], decreases monotonously with Ar-content in $CH_4/H_2/Ar$ plasma used for growing MCD layer to around 20–30 nm for MCD-UNCD$_5$ films [Fig. 2(c)]. Such a cauliflowerlike microstructure is significantly different from the faceted granular structure for MCD films (not shown) and ultrasmall equiaxed granular structure for UNCD films (cf. Fig. 1).

Raman spectroscopy of these MCD-UNCD$_n$ composite films is shown in Fig. 3(a), where the Raman spectra of MCD and UNCD films were also included to facilitate comparison. Typical Raman characteristics for materials with ultrasmall granular structure are observed for UNCD films, i.e., the UNCD Raman spectrum contains ν_1-band at 1140 cm^{-1} and ν_3-band at 1480 cm^{-1} resonance peaks, representing the transpolyacetylene locating at grain boundaries,[17,18] and D*-band at 1350 cm^{-1} and G-band at 1580 cm^{-1} resonance peaks, representing the disorder carbons and graphites.[19,20] In contrast, a sharp D-band at 1332 cm^{-1} is observed for MCD spectrum. The MCD-UNCD$_n$ composite films contain both of the features of MCD and UNCD films. The relative intensity of UNCD-related Raman resonance peaks increase with the Ar-content in the plasma used for growing the MCD layer.

Surprisingly, the MCD-UNCD composite films exhibit markedly superior EFE properties to the MCD films. Figure 3(b) shows that the turn-on field (E_0) needed for inducing the EFE process varies systematically with the Ar-content used for growing MCD layers. The E_0-value first decreases from 23.2 to 6.50 V/μm when the Ar-content in the plasma for growing MCD layer [x-value in $CH_4/H_2/Ar=1/(99-x)/x$] increases from 0 to 50 [curves 1~3, Fig. 3(b)]. The E_0-value then increases from 6.50 to 17.3 V/μm as the x-value increases from 50 to 90 [curves 3~5, Fig. 3(b)]. That is, the MCD-UNCD$_3$ films possess the best EFE properties among the composite films [$(E_0)_{UNCD3}$=6.5 V/μm]. Notably, the MCD-UNCD$_n$ (n=2, 3, or 4) films possess EFE properties, which are even better than that for UNCD films, i.e., $(E_0)_{MCD\text{-}UNCD_n}$=12.7–15.3 V/$\mu$m [curves 2~4, Fig. 3(b)] and $(E_0)_{UNCD}$=17.6 V/μm [curve 0_b, Fig. 3(b)], not mentioned the EFE of MCD films, which can be turned on at 27.0 V/μm [curve 0_a, Fig. 3(b)] These characteristics are

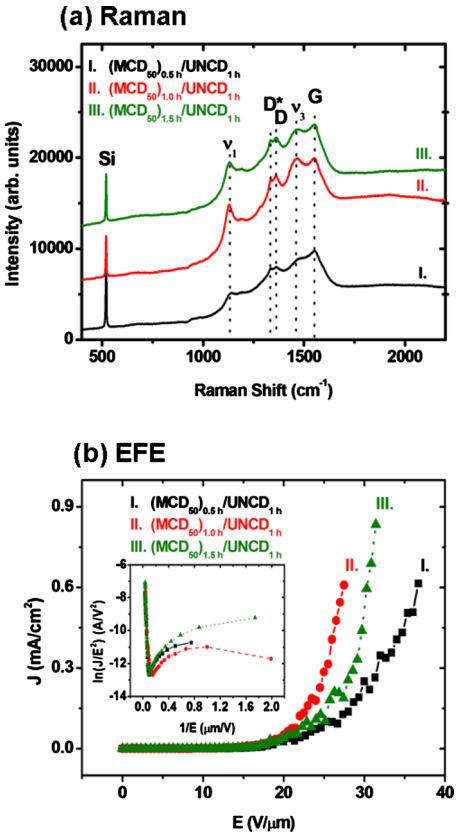

FIG. 4. (Color online) (a) Raman spectroscopy and (b) EFE properties for MCD-UNCD composite diamond films grown on UNCD nucleation layer, where the MCD layers were grown in $CH_4/H_2/Ar=1/49/50$ for (i) 30, (ii) 60, and (iii) 90 min.

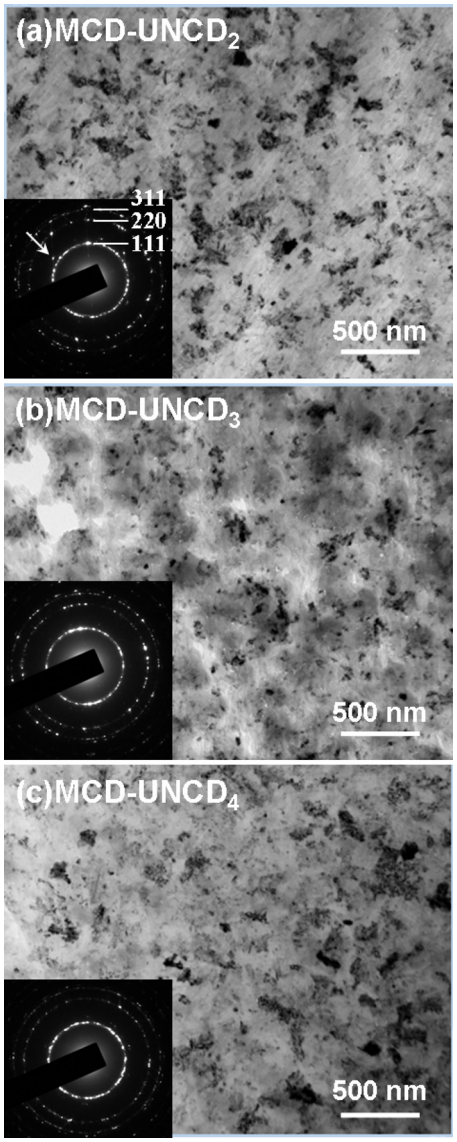

FIG. 5. (Color online) TEM microstructures for surface layer of MCD-UNCD composite diamond films grown on UNCD nucleation layer. The MCD layers were grown in $CH_4/H_2/Ar=1/(99-x)/x$ SCCM plasma with x=(a) 25 SCCM (MCD-$UNCD_2$), and (b) 50 SCCM (MCD-$UNCD_3$), and (c) 75 SCCM (MCD-$UNCD_4$) for 60 min (the insets show the corresponding SAED).

listed in Table I, revealing that the Ar-content in the plasma used for growing MCD layer influences profoundly the EFE properties of MCD-UNCD films.

In an attempt for further enhancing the EFE properties of the composite diamond films, the interval for growing secondary MCD layer was varied from 30, 60 to 90 min, using $CH_4/H_2/Ar=1/49/50$ plasma. The corresponding composite films were designated as MCD-$UNCD_{30}$, MCD-$UNCD_{60}$, and MCD-$UNCD_{90}$, respectively. The SEM morphology for these series of MCD-UNCD films is very similar with that of the first series of MCD-UNCD films [(cf. Fig. 2(b)], viz., they are of cauliflowerlike microstructure, containing large aggregates with fine structure on surface of the aggregates. Figure 4(a) shows that the Raman spectroscopy of this series of MCD-UNCD composite films also contain both of the features of MCD and UNCD films, viz., the Raman spectra contain ν_1-band (at 1140 cm^{-1}), ν_3-band (at 1480 cm^{-1}), D^*-band (at 1350 cm^{-1}), and G-band (at 1580 cm^{-1}) resonance peaks, representing the UNCD characteristics, and a sharp D-band (at 1332 cm^{-1}), representing the is MCD ones. Such a Raman spectroscopy insignificantly changes with the period for growing the MCD layer in MCD-UNCD films.

The EFE properties of this series of MCD-UNCD films are shown in Fig. 4(b) and the turn-on field extracted from these curves are listed in Table I. Interestingly, all the secondary series of MCD-UNCD films exhibit EFE properties superior to those of the UNCD films. The turn-on field (E_0) needed for inducing EFE process is smallest for MCD-$UNCD_{60}$ films that contain 60 min MCD layer [$(E_0)_{MCD\text{-}UNCD_{60}}$=6.5 V/$\mu$m, Fig. 4(b)]. These results indicate that the interval for growing MCD layer in $CH_4/H_2/Ar=1/49/50$ SCCM plasma on UNCD nucleation layer is also critical to induce appropriate granular structure for enhancing the EFE properties for MCD-UNCD composite materials.

The microstructure of the MCD-$UNCD_2$, MCD-$UNCD_3$, and MCD-$UNCD_4$ films, which exhibit better EFE properties than other films, was examined using TEM. Figure 5 shows that these diamond films contain numerous aggregates uniformly distributed in the samples, which is distinctly different from the faceted granular structure for MCD films and equiaxed granular structure for UNCD films. All the associated SAED (inset, Fig. 5) consists of diffraction rings corresponding to (111), (220), and (311) of cubic diamond lattices

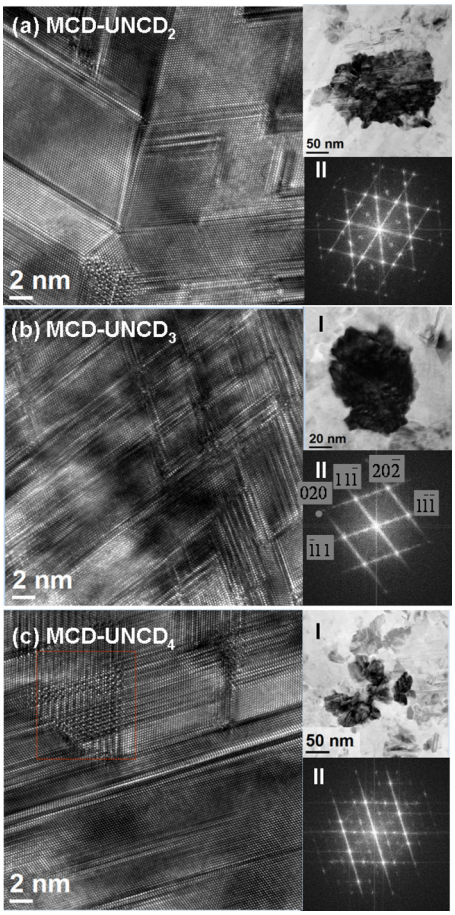

FIG. 6. (Color online) TEM structures for surface layer of MCD-UNCD composite diamond films grown on UNCD nucleation layer. The MCD layers were grown in $CH_4/H_2/Ar=1/(99-x)/x$ SCCM plasma with x=(a) 25 SCCM (MCD-$UNCD_2$), and (b) 50 SCCM (MCD-$UNCD_3$), and (c) 75 SCCM (MCD-$UNCD_4$) for 60 min (the inset I shows the low magnification bright field images from where the structure image was taken, whereas inset II shows the FT diffractograms corresponding to structure images).

(3C-diamond), along with a diffused ring in the central part of SAED, which corresponds to amorphous carbons. Detail analyses on the SAED reveal a subtle difference in the structure of the three films. First, the (311) and (220) rings of MCD-$UNCD_2$ films [inset, Fig. 5(a)] are relatively spotty, as compared with those of other films [insets, Figs. 5(b) and 5(c)], indicating that the grains in the aggregates of MCD-$UNCD_2$ films are larger in size and less populated than those in other films. Secondary, the intensity of the central diffused ring is larger for the MCD-$UNCD_3$ films, as compared with those of the other films, implying that MCD-$UNCD_3$ films contain larger proportion of amorphous carbon (or sp^2-bonded phase) than the other films. The significance of such observations will be further discussed shortly. Moreover, there exists n-diamond (FCC structured diamond) scarcely distributed in the matrix, which is indicated by extra spots outside (111) diffraction ring [arrowed, inset, Fig. 5(a)].

The enlarged microstructure of the large aggregates examined using high resolution TEM is shown in Fig. 6, indicating that all the films contain complicated microstructure. Inset I in Fig. 6 indicates that the size of aggregates decreased with the Ar-content in the plasma used for growing MCD layer, which is in accord with low magnification TEM micrographs shown in Fig. 5. The structure image corresponding to MCD-$UNCD_3$ films grown in $CH_4/H_2/Ar=1/49/50$ SCCM plasma [Fig. 6(b)] looks most complicated but Fourier-transformed (FT) diffractogram shows that the source of parallel fringes is actually simplest. There are streaks lying along $[1\bar{1}\bar{1}]$ and $[11\bar{1}]$ directions (inset II, Fig. 6(b)], indicating that the parallel fringes in Fig. 6(b) are the two variances of the edged-on image of stacking faults.[21] Figure 6(a) indicates that increasing the H_2-content in the plasma for growing the MCD layer markedly suppresses the formation of stacking faults but induces the presence of twining for MCD-$UNCD_2$ samples, whereas Fig. 6(c) shows that decreasing the H_2-content in the plasma for growing the MCD-$UNCD_4$ layer induces the appearance of hexagonal diamond polymorph (indicated by dotted squares),[21] in addition to the formation of stacking faults. However, the occurrence of complicated microstructure for large aggregates does not seem to be the main factor altering the EFE properties of these MCD-UNCD composite diamond films, as the aggregates in these films contain very few grain boundaries and cannot efficiently transport the electrons.

It is believed that the small-grain region in MCD-UNCD composite films is responsible for improving the EFE behavior for the films, as UNCD films are known to consist of large proportion of grain boundaries, which facilitate the transport of electrons and enhance the EFE properties.[22,23] The question remaining now is that if the UNCD region is the conducting channels for electrons in EFE process, how can the MCD-$UNCD_n$ films exhibit better EFE properties than the UNCD films. There must be some phases, which transport electrons better than the amorphous grain boundaries in UNCD materials for further enhancing their EFE properties. The microstructure of the small-grain region in MCD-$UNCD_3$ films were thus detailed examined for the purpose of understanding their role in enhancing the EFE for these composite films.

Figure 7(a) shows typical microstructure of a region near the large-grain in MCD-$UNCD_3$ films. It should be noted that in order to examine more clearly the microstructure of the interfacial region, the sample was tilted such that the aggregates are away from the zone axis and insignificantly diffract the electrons. The designated region (dotted squares) in Fig. 7(a) was further enlarged and was shown in Fig. 7(b) to clearly show the presence of ultrasmall diamond grains around 3–5 nm in size near the interfacial regions. Furthermore, the structure image reveals that, in addition to the commonly observed nanodiamond grains (area 1 and FT_1), there exists graphitic phase [area 2 and FT_2, Fig. 7(b)]. It is believed that the nanographites not only present in the region near the MCD-to-UNCD interface but also along the UNCD grain boundaries. Restated, the unique surface morphology observed in Fig. 2 for MCD-$UNCD_3$ composite films is actually the coexistence of large MCD grains with ultrasmall UNCD diamond grains, forming composite diamond. The nanographites are located along the boundaries of the grains and can form electron conduction path. Such a unique granular structure is presumed to be the cause, resulting in en-

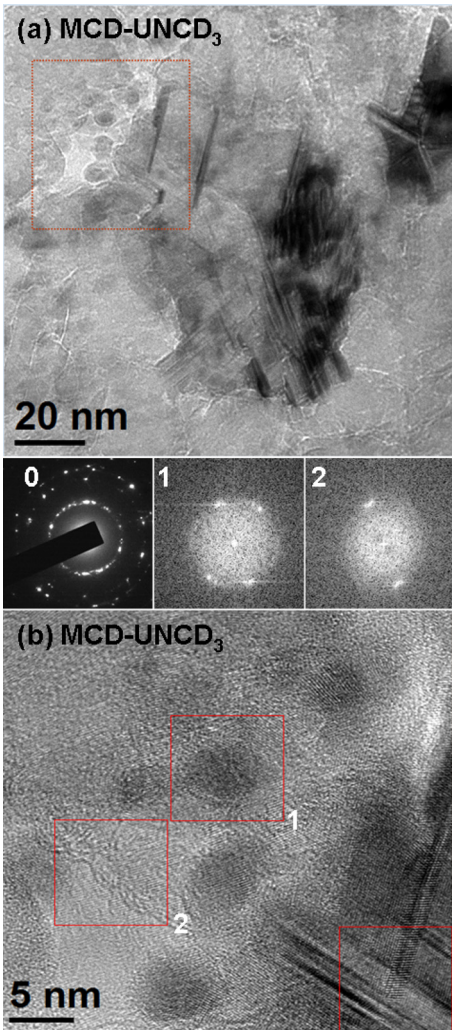

FIG. 7. (Color online) (a) TEM micrograph for surface layer of MCD-$UNCD_3$ composite diamond films grown on UNCD nucleation layer with the SAED shown as inset "0." The MCD and UNCD layers were grown in $CH_4/H_2/Ar=1/49/50$ SCCM and 4/0/196 SCCM plasma, respectively; (b) the structure image corresponding to the regions designated in (a). The insets, FT_1 and FT_2, show FT diffractograms corresponding to the designated areas 1 and 2.

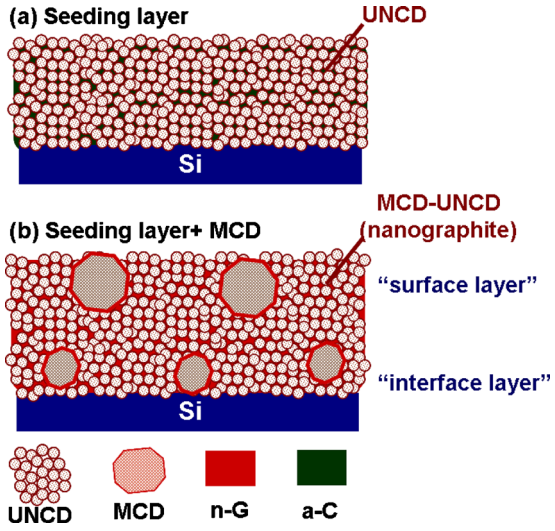

FIG. 8. (Color online) The schematic diagram for the microstructural evolution of MCD-UNCD composite films: (a) the UNCD nucleation layer containing ultrasmall grains and (b) the MPECVD process induced the coalescence of nanosized grains to form large aggregates, in conjunction with the induction of nanographites.

hanced EFE for the MCD-UNCD composite materials, as the nanographite is more conductive than the amorphous carbons in the UNCD grain boundaries.

The constituent in the $CH_4/H_2/Ar$ plasma for growing the MCD layer on UNCD nucleating layer is critical in inducing such a unique microstructure. Too large proportion of H_2 in the plasma may induce too abundant atomic hydrogen, which will etch out amorphous carbon in the grain boundaries, suppressing the formation of nanographites and lowers the EFE properties for the composite films. In contrast, too little proportion of H_2 in the plasma cannot trigger the transformation of amorphous carbons in the grain boundaries into nanographites. Only when the MCD films were grown in plasma of proper $CH_4/H_2/Ar$ composition, can the graphitic phase be induced, locating in the grain boundaries and enhancing the EFE properties of the composite films. Such a growth mechanism accounts for the EFE behavior of first series of MCD-UNCD composite films very well.

Notably, the two-step process does not grow micron-sized grains on top of UNCD. Instead, the second step of MPECVD process converted the equiaxed granular structure of UNCD layer into large-grain/ultrasmall-grain composite microstructure. The large grains, approximately hundreds of nanometers in size, not only exist in the top layer of the MCD-UNCD samples but also present in the bottom layer of the samples. Such an argument is schematically illustrated in Fig. 8 and will be demonstrated by examining the microstructure of "surface layer" and "interface layer" of MCD-UNCD films shortly. It should be reminded that, in the conventional process for growing UNCD films, the growth of secondary diamond layer were proceeded in hydrogen free plasma (Ar/CH_4) on seeding layer. The grains will be maintained in nanosize even for a film with tens of micron in thickness, i.e., it will not induce the increase in grain size. Such a phenomenon is schematically illustrated in Fig. 8(a). The grain boundaries in such a film is mainly disordered carbons (or amorphous carbons),[17,18] which are represented as green background in Fig. 8(a).

During the preparation of thin foil for TEM examination, we can ion-mill the samples from the Si-side, resulting in a thin foil containing mostly the surface layer of the MCD-UNCD samples (designated as surface layer). Figures 5–7 show the microstructure of the surface layer of MCD-$UNCD_3$ samples, which consist of nanosized spherical grains (~5 nm), coexisting with large aggregates (hundreds of nanometers). On the other hand, we can ion-mill the samples from the surface side, resulting in a thin foil containing mostly the materials near the MCD-UNCD to Si interface region (designated as interface layer). Interestingly, the large aggregates were also observed in the interface layers of these composite samples, which are schematically illustrated in Fig. 8(b).

Figure 9(a) shows a typical TEM micrograph of the interface layer of MCD-$UNCD_3$ films, revealing the presence of large aggregates distributed among the small-grains matrix. SAED shown in the inset of Fig. 9(a) indicates that the

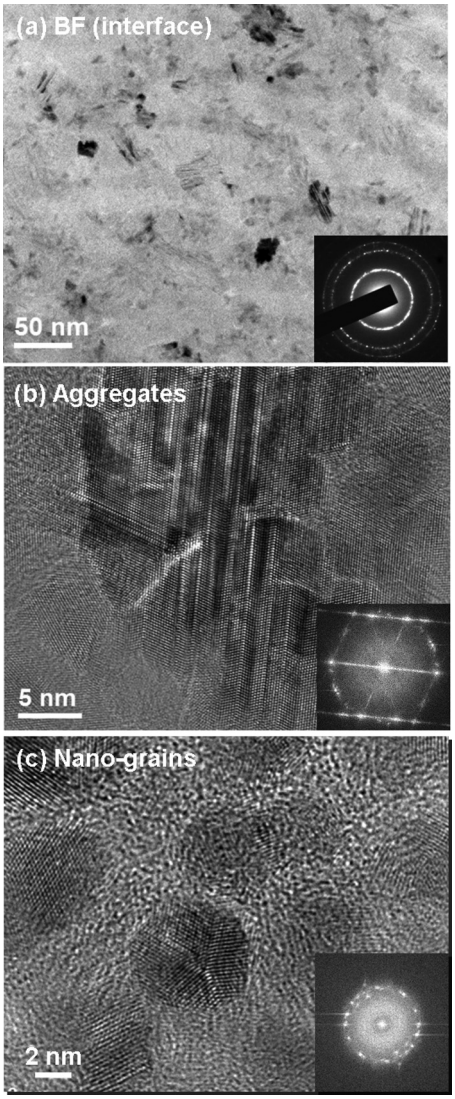

FIG. 9. The (a) low magnification TEM image, and [(b) and (c)] structure image of the large aggregate region (b) and small-grain region (c) of the MCD-UNCD films near the film-to-substrate interface region, i.e., interface layer.

films are of diamond structure (3C-diamond). Detailed analysis on SAED reveals a subtle difference in microstructure of interface layer from that of surface layer, viz., the interface layer does not contain n-diamond, as there is no extra spots outside (111) diffraction ring [cf. Figs. 5(a)–5(c)]. The implication of such an observation is that the Oswald ripening process occurs less rigorous in the interface layer, as compared with that in surface layer, as n-diamond usually occurs in accompanying the coalescence of nanosized grain into large aggregates.[15,24]

Figures 9(b) and 9(c) show structure image of large aggregates and small-grain areas in interface layer, respectively. The large aggregates [Fig. 9(b)] also consist of faulted diamonds, which is implied by the presence of parallel fringes in structure image and the streaks in the FT-diffractograms [inset, Fig. 9(b)]. However, the large aggregates in interface layer are much less defective than those in surface layer (cf. Fig. 6). Such an observation infers, again, that the coalescence phenomenon of diamond grains in interface layer is not as rigorous as that in surface layer. Moreover, the small grain area consists of spherical grains about 5 nm in size and is uniformly distributed [Fig. 9(c)]. There also exist grain boundaries about 1–2 nm in thickness. The central ring in the diffractogram in Fig. 9(c) infers that the grain boundaries contain large proportion of nanographites, which cannot be clearly resolved in structure image. Apparently, the large aggregates are formed by Oswald ripening process. The proportion of large aggregates is smaller in the interface layer, as compared with those in the surface layer. The nanographites are expected to be induced as a result of coalescence of nanosized grains.

The presence of nanographites in both interface layer and surface layers will form electron interconnecting channels through the thickness of the samples and pronouncedly enhance the EFE properties of the MCD-UNCD materials. Too short deposition interval for the second MPECVD process can only lead to coalescence process for the surface layer but will not be able to induce the coalescence process for the interface layer and cannot results in the formation of nanographites in this region. On the other hand, too long deposition interval for the second MPECVD process will result in a large grain layer, completely covering the top of MCD-UNCD films. Both cases lead to a resistive layer connected to the conducting MCD-UNCD composite layer in series that will degrade the EFE process. Such a growth mechanism can account for the EFE behavior for the second series of MCD-UNCD composite films very well.

Moreover, the presence of amorphous carbon in UNCD nucleation layer is also very critical in the formation of proper microstructure for enhancing EFE properties for MCD-UNCD composite materials. Separated experiments (not shown) indicated that when the UNCD nucleating layer was grown in Ar/CH_4 plasma containing a few percentage of H_2 ($<3\%$), the amorphous carbon in the grain boundaries of UNCD films will be eliminated and the UNCD nucleating layer is insulating. The growth of secondary MCD layer can also form large-grain/small-grain composite material but will not enhance the EFE properties.

IV. CONCLUSION

MCD-UNCD composite films exhibiting superior EFE properties to MCD or UNCD films were successfully synthesized by growing a secondary diamond films on a UNCD nucleation layer. Both the Ar/H_2 ratio and deposition time used for growing secondary diamond layer markedly influence the EFE properties of the resulted MCD-UNCD composite films. Microstructure examinations using high resolution TEM shows that the MCD-UNCD composite diamond films consist of microsized grains, about hundreds of nanometer in size, surrounded by the ultrasmall grains, about 5 nm in size. The secondary MPECVD process modifies the granular structure of the UNCD films, instead of forming a micron-sized granular structured diamond films on top of UNCD films. The presence of nanographites in the interfacial region between the grains is presumed to be the prime factor resulting in superior EFE properties for MCD-UNCD films. The EFE of these MCD-UNCD composite diamond

films can be turned on at a low field as 6.5 $V/\mu m$ and attain large EFE current density about 1.0 mA/cm^2 at 30 $V/\mu m$ applied field. Such an EFE characteristic is superior to the nondoped planar diamond films ever been reported.

ACKNOWLEDGMENTS

The authors would like to thank the National Science Council, Republic of China for the support of this research through the Project No. NSC 99-2119-M-032-003-MY2.

[1]K. Chakrabarti, R. Chakrabarrti, K. K. Chattopadhyay, S. Chaudhrui, and A. K. Pal, Diamond Relat. Mater. **7**, 845 (1998).
[2]V. Ralchenko, A. Karabutov, I. Vlasov, V. Frolov, V. Konov, S. Gordeev, S. Zhukov, and A. Dementjev, Diamond Relat. Mater. **8**, 1496 (1999).
[3]S. G. Wang, Q. Zhan, S. F. Yoon, J. Ahn, Q. Wang, Q. Zhou, and D. J. Yang, Phys. Status Solidi A **193**, 546 (2002).
[4]D. M. Gruen, Annu. Rev. Mater. Sci. **29**, 211 (1999).
[5]J. A. Carlisle and O. Auciello, Electrochem. Soc. Interface **12**, 28 (2003).
[6]V. Mortet, O. Elmazria, M. Nesladek, M. B. Assouar, G. Vanhoyland, J. D'Haen, M. D. Olieslaeger, and P. Alnot, Appl. Phys. Lett. **81**, 1720 (2002).
[7]W. Zhu, G. P. Kochanski, and S. Jin, Science **282**, 1471 (1998).
[8]Y. C. Lee, S. J. Lin, C. T. Chia, H. F. Cheng, and I. N. Lin, Diamond Relat. Mater. **13**, 2100 (2004).
[9]T. D. Corrigan, D. M. Gruen, A. R. Krauss, P. Zapoa, and R. P. H. Chang, Diamond Relat. Mater. **11**, 43 (2002).
[10]A. R. Krauss, O. Auciello, M. Q. Ding, D. M. Gruen, Y. Huang, V. V. Zhirnov, E. I. Givargizov, A. Breskin, R. Chechen, E. Shefer, V. Konov, S. Pimenov, A. Karabutov, A. Rakhimov, and N. Suetin, J. Appl. Phys. **89**, 2958 (2001).
[11]S. Bhattacharyya, O. Auciello, J. Birrell, J. A. Carlisle, L. A. Curtiss, A. N. Goyette, D. M. Gruen, A. R. Krauss, J. Schlueter, A. Sumant, and P. Zapol, Appl. Phys. Lett. **79**, 1441 (2001).
[12]O. A. Williams, S. Curat, J. E. Gerbi, D. M. Gruen, and R. B. Jackman, Appl. Phys. Lett. **85**, 1680 (2004).
[13]P. T. Joseph, N. H. Tai, and I. N. Lin, Appl. Phys. Lett. **97**, 042107 (2010).
[14]C. S. Wang, H. C. Chen, H. F. Cheng, and I. N. Lin, Diamond Relat. Mater. **18**, 136 (2009).
[15]C. S. Wang, H. C. Chen, H. F. Cheng, and I. N. Lin, J. Appl. Phys. **105**, 124311 (2009).
[16]R. H. Fowler and L. Nordheim, Proc. R. Soc. London, Ser. A **119**, 173 (1928).
[17]A. C. Ferrari and J. Robertson, Phys. Rev. B **63**, 121405 (2001).
[18]R. G. Buckley, T. D. Moustakas, L. Ye, and J. Varon, J. Appl. Phys. **66**, 3595 (1989).
[19]J. Michler, Y. Von Kaenel, J. Stiegler, and E. Blank, J. Appl. Phys. **83**, 187 (1998).
[20]A. C. Ferrari and J. Robertson, Phys. Rev. B **61**, 14095 (2000).
[21]I. N. Lin, H. C. Chen, C. S. Wang, Y. R. Lee, and C. Y. Lee, private communication.
[22]Y. C. Lee, S. J. Lin, D. Pradhan, and I. N. Lin, Diamond Relat. Mater. **15**, 353 (2006).
[23]Y. C. Lee, S. J. Lin, I. N. Lin, and H. F. Cheng, J. Appl. Phys. **97**, 054310 (2005).
[24]B. G. Burkhard, K. Dan, Y. Tanabe, A. K. Sawaoka, and K. Yamada, J. Appl. Phys. **33**, 5875 (1994).